

# Non-Uniform Strain Engineering of 2D Materials

Sviatoslav Kovalchuk<sup>+</sup>,<sup>[a]</sup> Jan. N. Kirchhof<sup>+</sup>,<sup>[a]</sup> Kirill I. Bolotin,<sup>[a]</sup> and Moshe G. Harats<sup>\*[b]</sup>

**Abstract:** 2D materials are elastic substances that can sustain high strain. While the response of these materials to spatially uniform strain is well studied, the effects of spatially non-uniform strain are understood much less. In this review, we examine the response of two different 2D materials, transition metal dichalcogenides and graphene, under non-uniform strain. First, we analyze pseudo-magnetic fields formed in graphene subjected to highly localized non-uniform strain. Second, we discuss the effect of non-uniform

strain on excitons in non-uniformly strained TMDC. We show that while transport or “funneling” of excitons is relatively inefficient, a different process, a strain-related conversion of excitons to trions is dominant. Finally, we discuss the effects of uniform and non-uniform strain in a graphene-based phononic crystal. We find that uniform strain can be used to broadly tune the frequency of the phononic bandgap by more than 350% and non-uniform strain smears that bandgap.

**Keywords:** 2D materials · Non-uniform strain · Funneling · Phononic crystal

## 1. Introduction

Two-dimensional materials such as graphene, a semi-metal, and transition metal dichalcogenides (TMDCs), semiconductors in the 2H phase, are attractive candidates for future flexible electronics applications.<sup>[1]</sup> They feature a high breaking strain limit of  $> 10\%$ <sup>[2,3]</sup> and are very stiff at the same time, with Young's modulus of up to 250 *GPa*<sup>[2]</sup> for TMDCs and up to 1 *TPa* in graphene.<sup>[3]</sup> Their flexibility, elasticity and high strength makes them prime candidates for tunable optoelectronic devices. Strain engineering has been used to control the size and the nature of the bandgap, break symmetries, control phonons and scattering in these materials.<sup>[1,4,5]</sup> The majority of the studies so far considered the effects of spatially uniform strain. At the same time, relatively unstudied spatially non-uniform strain produces several new classes of physical phenomena. The most celebrated effect of spatially non-uniform strain is the generation of a pseudo-magnetic field in non-uniformly strained graphene.<sup>[6,7]</sup> It has been shown that a varying strain profile has the same effect on the system's Hamiltonian as an external magnetic field – with the difference that it has an opposite sign for *K* and *K'* valley electrons. Signatures of Quantum Hall-like effects in such a field have been observed.<sup>[6,7]</sup> In another example, a pioneering theoretical study predicted that non-uniform strain drives transport of normally charge neutral bosonic particles, excitons, in TMDCs.<sup>[8]</sup> Such an effect has been suggested as a tool to increase the efficiency of photoconversion.

Here, we review the use of non-uniform strain as a control knob for exploiting and manipulating different degrees of freedom of 2D materials. Our specific focus is the effect of non-uniform strain on dynamics of excitons in TMDCs and phonons in a graphene phononic crystals.

## 2. Uniform Strain

We start by briefly summarizing much more studied effects of spatially uniform strain on excitons in TMDCs and phonons in graphene. For a more detailed discussion of these effects, an excellent review focusing on uniform strain is available<sup>[1]</sup> with an additional review covering also inhomogeneous strain can be found in Ref. [9]

### 2.1 Uniform Strain in TMDCs

One straightforward way to achieve controllable uniaxial strain is by placing a TMDC on a flexible substrate that is then strained in the four-point bending apparatus.<sup>[4]</sup> The strain changes the orbital overlap between neighboring atomic sites (see Figure 1a) affecting the optical bandgap (that can be probed via photoluminescence measurements) and the phonon frequencies (probed via Raman spectroscopy). Both valence and conduction bands react to applied strain.<sup>[10,11]</sup> In the case of a uniform strain, the energy levels are continuously down-

[a] S. Kovalchuk,<sup>+</sup> J. N. Kirchhof,<sup>+</sup> K. I. Bolotin  
Department of Physics,  
Freie University Berlin  
14195 Berlin, Germany

[b] M. G. Harats  
Department of Materials Engineering,  
Ben Gurion University  
84105 Be'er Sheva, Israel  
E-mail: mharats@bgu.ac.il

[<sup>+</sup>] Authors contributed equally

© 2022 The Authors. Israel Journal of Chemistry published by Wiley-VCH GmbH. This is an open access article under the terms of the Creative Commons Attribution License, which permits use, distribution and reproduction in any medium, provided the original work is properly cited.

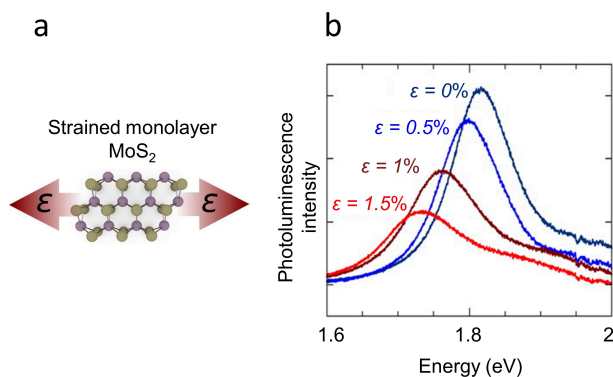


**Figure 1.** (a) A schematic drawing of the distorted hexagonal lattice of a typical TMDCs under uniaxial strain. (b) PL spectra as a function of strain for a uniaxial strained MoS<sub>2</sub> monolayer. The exciton peak is red-shifted and drops in intensity as a function of strain. Reproduced with permission from Ref. [4].

shifted which results in reduction of the bandgap by  $\sim 50$  meV/% for uniaxial strain<sup>[4,5]</sup> and  $\sim 100$  meV/% for biaxial strain,<sup>[12]</sup> both values for MoS<sub>2</sub>. Figure 1b presents the change in the photoluminescence (PL) spectrum of monolayer MoS<sub>2</sub> under strain. The size of the optical bandgap can be read out from the position of the PL peak (A exciton). The shift of the peak is consistent with the predicted rate of bandgap downshift of  $\sim 50$  meV/%.<sup>[4,5]</sup> An additional visible feature is the decreasing PL intensity as a function of strain. This feature arises from the changes in the TMDCs band structure. Indeed, in MoS<sub>2</sub>, the indirect bandgap has higher strain sensitivity ( $\sim 94$  meV/%) compared to the direct

bandgap. At high enough strain the character of MoS<sub>2</sub> bandgap transforms from direct to indirect.<sup>[4]</sup> Uniaxial strain also changes the phonon spectra, resulting in the splitting of the *E* Raman peak into two distinctive modes with strain-dependent frequency separation.<sup>[4]</sup>

## 2.2 Uniform Strain in Phononic Crystals

After achieving major technological breakthroughs by controlling photons and electrons in the past decades, now the phonon is receiving more and more attention. To control phonons, one needs an artificial structure with periodically varying mechanical potential – a so called phononic crystal.<sup>[13]</sup> Typically, a phononic crystal is created by periodically modulating mass, density or strain of the material.<sup>[12]</sup> Analogous to Bloch-electrons in a solid, there is a phononic band structure, which determines the energy of phonons travelling through the artificial crystal.<sup>[13,14]</sup> This now can be used to guide<sup>[15–17]</sup> and focus phonons<sup>[18–20]</sup> or to open a vibrational bandgap.<sup>[13,19,20]</sup> Typically, phononic crystals are made from stiff materials such as silicon<sup>[21]</sup> or silicon nitride,<sup>[22,23]</sup> which do not provide necessary flexibility to introduce non-uniform strain. If, however, the phononic crystal is made from a flexible 2D material such as graphene, strain tuning becomes a fruitful option.

In Figure 2a, we show a recently considered graphene phononic crystal.<sup>[24]</sup> He-Ion lithography is used to cut a honeycomb lattice of holes creating the phononic order.<sup>[25]</sup> The unit cell of the artificial lattice and the corresponding Brillouin zone are shown in Figure 2b. The phononic band structure as



Sviatoslav Kovalchuk received his BSc and MSc from Moscow University of Physics and Technology in 2012 and 2015. In 2017 he moved to Freie Universität Berlin, joining the group of Prof. Bolotin, and since has worked on the strain in 2D materials, CVD growth of graphene and TMDCs, molecular deposition on 2D materials. Currently pursuing his PhD, focusing on the topic of organic-inorganic interfaces in 2D materials.



Jan Niklas Kirchhof received his BSc and MSc in Physics from the RWTH Aachen University in 2014 and 2016. During his master thesis he studied mechanical resonators made from graphene in the group for Prof. Stampfer. He then continued to investigate the dynamics of 2-dimensional materials in the group of Prof. Bolotin at Freie Universität in Berlin, where he is pursuing his PhD. Currently he is working on phononic systems and nano-mechanics of 2-dimensional membranes under strain.



Kirill Bolotin works in the field of electron transport and optoelectronics of two-dimensional materials. He holds the chair of electrical transport in 2D materials. He was involved in the discovery of the fractional quantum effect in graphene, the demonstration of strain-engineering of 2D MoS<sub>2</sub>, first measurements of the exciton binding energy in 2D MoS<sub>2</sub>, and the discovery of the renormalization of the elastic constants of the 2D materials. He was awarded the US NSF Career award (2010), the Sloan foundation award (2011), and the ERC starting grant (2016).



Moshe G. Harats has received his BSc, MSc and PhD from the Hebrew University of Jerusalem in Physics. During his PhD he has shown coupling of a single nanocrystal quantum dot to a plasmonic nanoantenna with high collection efficiency at room temperature. In his postdoc at Freie University in Berlin, he specialized in straining 2D materials with a home-built AFM along with optical spectroscopy. He is currently an assistant Professor at the Department of Materials Engineering at Ben Gurion University.

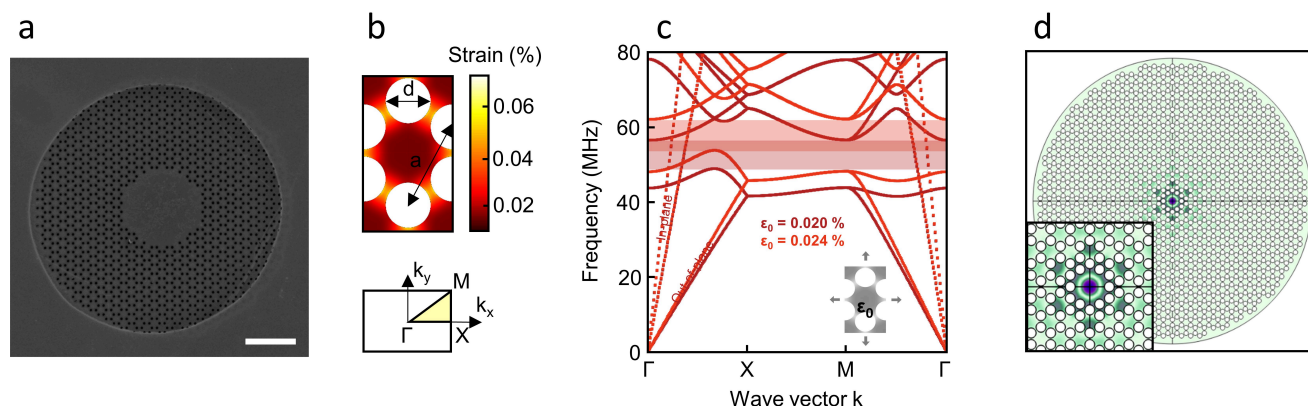


**Figure 2.** Graphene phononic crystal. (a) Helium ion micrograph of a prototype suspended monolayer graphene phononic crystal device with lattice constant  $a=350$  nm (scale bar length is  $2 \mu\text{m}$ ). The phononic pattern consists of a honeycomb lattice of holes. The defect in its center is used to localize a vibrational defect mode. (b) Crystal unit cell for the honeycomb lattice with redistributed strain (top) and the matching first Brillouin zone (bottom). (c) Phononic band structure for two different values of pre-strain and the lattice from (b). Out-of-plane modes plotted as solid lines, in-plane modes as dashed lines. Around 50 MHz there is a quasi-bandgap region for out of plane modes (red-shaded area). (d) The defect mode localized in the center of the phononic device. Inset shows a zoom-in. Reproduced with permission from Ref. [24].

plotted in Figure 2c. A vibrational bandgap of around 50 MHz is visible for out-of-plane modes (solid lines). Within the bandgap the propagation of incoming waves is exponentially damped. This property was used to localize vibrational modes of frequency  $f$ . Such a localized mode is similar to a defect state within a bandgap of a semiconductor. In Figure 2d, we show the mechanical equivalent: a localized oscillation in the center of the device. This mode is shielded from the environment by the phononic patterning surrounding it and is expected to show a resonance of narrow linewidth  $\Delta f$  (high  $Q = f/\Delta f$ ).

The key advantage of such a graphene phononic device is its mechanical tunability. When the device is strained, its vibrational frequencies upshift – similar to tuning of a guitar string. To investigate the effect of uniform strain, we show the band structure for two different values of initial strain  $\epsilon_0$  (Figure 2c). We observe a uniform upscaling of all phonon branches and a corresponding upshift of the band gap. It is important to remark that the phononic order remains completely intact and the phononic bandgap stays unperturbed. From the band structure one can extract the group velocity (the speed of sound):

$$v_g = \frac{\partial \omega}{\partial k} \quad (1)$$

The data of Figure 2c suggests that straining increases the  $v_g$ . This implies that strain-tuning in flexible phononic crystals allows to control the speed at which information and heat travel through the material. At the same, spatially uniform strain does not affect the presence and the character of the phononic bandgap.

### 3. Spatially Non-Uniform Strain

After briefly reviewing the effects of spatially uniform strain, we focus on spatially non-uniform strain engineering as a new experimental approach to control material properties. In the case of TMDCs, free electrons, excitons, and trions can be guided (or “funneled”) by non-uniform strain.<sup>[8]</sup> It is especially interesting that non-uniform strain can be used to design a potential landscape where charge neutral excitons, which cannot be transported by means of electric fields (as they are neutral), can be transported to and accumulated at the point of highest strain corresponding to the point of the smallest bandgap.<sup>[8]</sup> Early pioneering works reported such funneling in multilayer  $\text{MoS}_2$ <sup>[26]</sup> and nanobubbles of  $\text{MoS}_2$ .<sup>[27]</sup>

Unfortunately, funneling is limited to small regions, which explains why it is observed only in wrinkles and nanobubbles. In addition, this process is limited by the thermodynamics that balances between the diffusion of the excitons and the drift that guides the excitons to the point of high strain.

#### 3.1 The Approaches to Generate Non-Uniform Strain

We review three different methods to generate non-uniform strain. The first setup is based on straining a clamped, suspended TMDC, with an AFM tip (Figure 3a). This method is called nanoindentation and is commonly used in the determination of the elastic properties of thin 2D materials.<sup>[3,28,31,32]</sup> The second route takes advantage of the fact that 2D materials are impregnable to air and can be pressurized by injecting gas under the surface of the suspended clamped 2D material<sup>[12]</sup> (Figure 3b). The third method strains the membrane by an electrostatic pressure produced when voltage is applied between a suspended graphene membrane and a

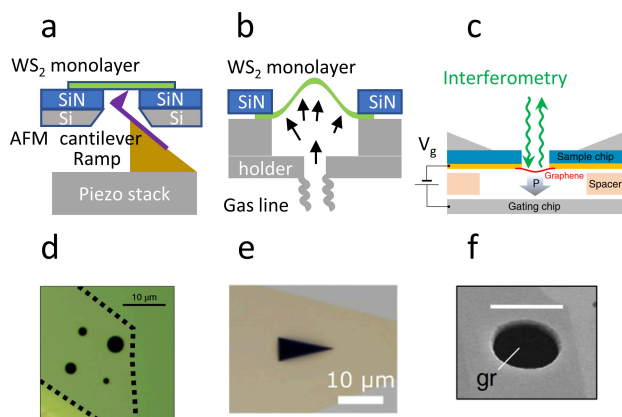


**Figure 3.** Experimental setups for induction of non-uniform strain. (a) Strain induction by in-situ AFM nanindentation. Monolayer WS<sub>2</sub> sample suspended over circular holes in SiN are used for this experiment is shown in (d). (b) Strain induction using pressurized gas. Monolayer WS<sub>2</sub> sample suspended over a triangular hole in SiN is shown in (e). (c) Strain induction by electrostatic pressure. A monolayer graphene sample suspended over a circular hole used here is shown in (f). Sub-figures a,d reproduced with permission from Ref. [28]. Sub-figures b,e reproduced with permission from Ref. [29]. Sub-figures c,f reproduced with permission from Ref. [30].

close-by electrode (Figure 3c). Additional methods to create non-uniform strain are nano-domes that occur naturally between TMDC and the underlying substrate,<sup>[27]</sup> and in an engineered manner where the nano-domes can be arranged in arrays.<sup>[33,34]</sup>

The samples for all three approaches were fabricated by drilling a hole in a SiN membrane with a focused-ion-beam (FIB)<sup>[16]</sup> and dry-transferring a WS<sub>2</sub> or graphene monolayers onto it. This creates a clamped monolayer covering a well-defined hole (see Figure 3d–f).

The nanindentation setup requires a home-built AFM due to the special need to strain the suspended monolayer from one side and excite and collect the PL from the other side. This system uses piezo-resistive tips<sup>[35]</sup> and operates either in vacuum or in air.<sup>[28]</sup> The AFM tip is mounted on a piezo stack and can perform both nanindentation and hold a constant force to allow long optical scans of the samples, at ambient and cryogenic temperatures. When the AFM performs a force-distance (nanindentation) experiment, the strain can be as high as 16%<sup>[28]</sup> but only for a short period. For long experiments which involve optical scans the strain is limited to < 4% due to rupturing of the samples. Next to the AFM tip the strain is highly non-uniform > 2%/μm.

In the second approach, we used gas pressure to strain the sample.<sup>[12,36,37]</sup> The strain non-uniformity is determined by the geometry of the hole over which the material is suspended. While circular holes require high pressure to achieve non-uniformity, samples suspended over holes with other shapes rupture easily. We found that uneven triangle shaped holes (sides of 5 μm and 12 μm) to be a good candidate, with the

strong non-uniformity of > 0.28%/μm, and withstanding strain values of > 2% at the center.<sup>[29]</sup>

In the third method, strain is induced electrostatically. This is done by applying a voltage between a suspended membrane and an electrode close to it. The highly conductive graphene and the gate electrode form a plate capacitor. The applied voltage produces an electrostatic pressure  $P$  acting on the membrane:

$$P = \frac{\epsilon_0}{2} E^2 \quad (2)$$

where  $E$  is the electric field and  $\epsilon_0$  is the vacuum permittivity. This pressure causes out-of-plane deformation for a graphene membrane as shown in Figure 3c. In a circular geometry (Figure 3f) the out-of-plane displacement naturally generates a non-uniform strain distribution within the device. With increasing applied electrostatic pressure, the global average strain rises, and the strain distribution becomes increasingly non-uniform, yet compared to the other presented methods, electrostatically strained samples typically show a more uniform strain distribution. This can be potentially controlled by changing the hole geometry similar to the previous method. One crucial difference, however, is that by applying electrostatic gate, the carrier density changes together with induced strain. This may be important for example in TMDCs, where both effects compete in PL response, as will be shown further.

### 3.2 Pseudo Magnetic Fields in Non-Uniformly Strained Graphene

Before focusing on the effects of non-uniform strain in TMDCs and phononic crystals, we briefly review the most celebrated effect of that strain – the generation of pseudomagnetic fields in graphene. The electrons in non-uniformly strain graphene behave as if they were exposed to an external magnetic field, giving rise to the name of the effect. Mathematically the strained system is described by the following Hamiltonian:

$$H = \hbar v_f \boldsymbol{\sigma} \cdot (\mathbf{k} - e\mathbf{A}) \quad (3)$$

where  $v_f$  is the Fermi velocity of graphene,  $\boldsymbol{\sigma}$  are the Pauli matrices,  $e$  is the elementary charge and  $\mathbf{A}$  is the gauge field defined as:

$$\mathbf{A} = \pm \frac{\beta}{a} \begin{pmatrix} u_{xx} - u_{yy} \\ -2u_{xy} \end{pmatrix} \quad (4)$$

Here  $a$  is the lattice constant,  $\beta$  is defined as  $-\frac{\partial \ln t}{\partial \ln a}$  and of the order of unity, and  $u_{ij} = \frac{1}{2} \left( \frac{\partial u_i}{\partial j} + \frac{\partial u_j}{\partial i} \right)$  for  $i, j = (x, y)$  is the deformation tensor.<sup>[6]</sup> From these equations one can see that spatially uniform strain leads to zero pseudo-magnetic fields and that non-uniform shear strain is needed to generate them.

Interestingly, the vector potential due to strain looks exactly like the potential due to a real field, at least in a single K valley. Therefore, sufficiently strong pseudo-magnetic field would cause the electrons to circulate and form Landau levels – very much like for a regular external magnetic field with difference that electrons in the K and K' valley circulate in opposite direction. The Landau quantization results in quantized electron conductivity in graphene, similar to what is observed in the quantum Hall effect, yet in the absence of an external magnetic field. However, it is experimentally very challenging to measure pseudo-magnetic field due to the unconventional geometry needed to generate the uniform pseudomagnetic fields.<sup>[7,38]</sup> This limited the observation of pseudo-magnetic fields to STM measurements<sup>[39–42]</sup> but neither electrical transport measurements nor more indirect signatures such as magneto-phonon resonances at  $B = 0$  are reported in literature. Nevertheless, there is experimental confirmation of pseudo-magnetic fields on a smaller scale found in STM measurements on graphene nanobubbles,<sup>[39]</sup> nanopillars,<sup>[40]</sup> tetrahedron nanoparticles,<sup>[42]</sup> and buckled graphene.<sup>[41]</sup> In these measurements Landau levels were observed and the corresponding pseudo magnetic field was determined to reach an astonishing value of more than 300 T, which stems from the very large variation of strain over the size of a nanoobject.<sup>[39]</sup>

### 3.3 Exciton and Electron Funneling in TMDCs

To investigate the role of non-uniform strain on the dynamics of excitons in TMDCs, we performed experiments with the setups depicted in Figure 3a,b. Figure 4a,d presents the evolution of the photoluminescence spectra as the strain is increased at the center of the samples, for both the nanoindentation (Figure 4a) and the pressurization (Figure 4d) setups. In both setups we observe the expected red-shift of the PL resulting from the decreasing bandgap as discussed earlier for the case of uniform strain (Figure 1b). However, the PL spectra do not show signatures of exciton funneling towards the point of the highest strain. Instead, we observe the emergence of a two-peak structure in the PL spectra (Figure 4a,d). Careful analysis of the structure shows that the lineshape cannot be explained by neutral 'A' exciton transition only, as was done in the uniform strain case. We attribute the second peak, redshifted vs. the A exciton, to the charged exciton (trion).<sup>[27,28]</sup> Trion is a quasiparticle created by binding of exciton and electron (or hole), and in WS<sub>2</sub> has a binding energy of  $\sim 30$  meV.<sup>[43]</sup> This is consistent with the observed peaks separation.<sup>[27,28]</sup> The rise of the trion peak with the strain is seen clearly for the case of nanoindentation where we perform an area scan and observe that the trion/exciton ratio increases dramatically at the center of the suspended 2D material (see Figure 4b).

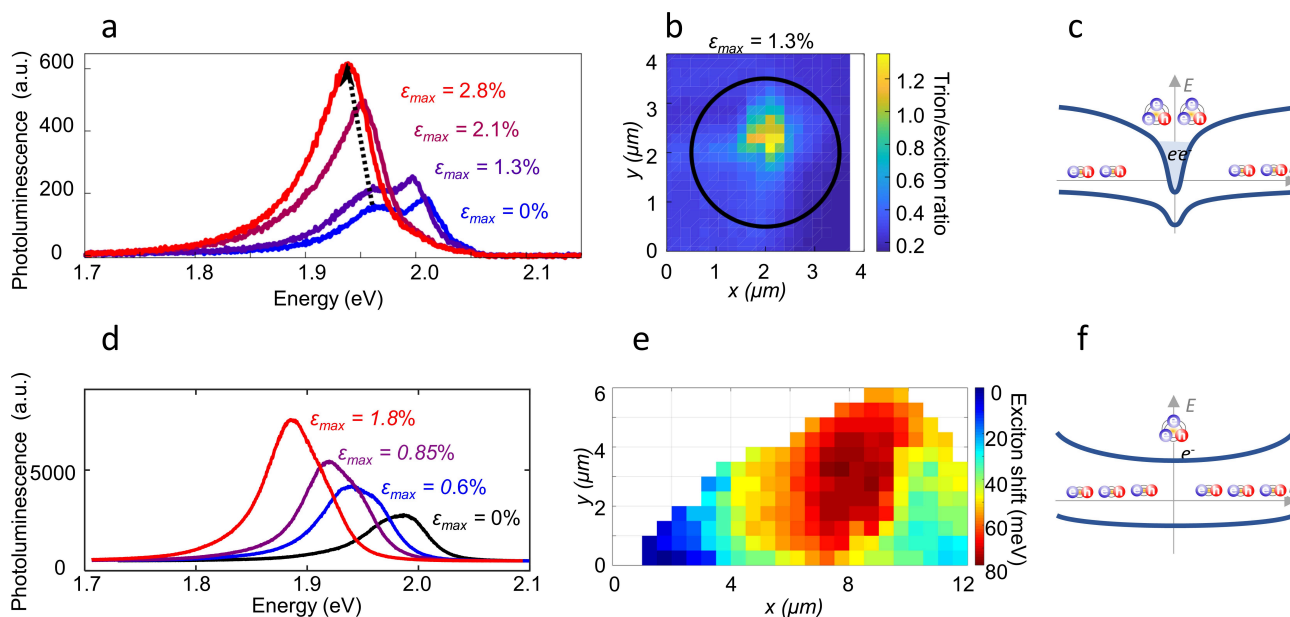


**Figure 4.** Experimental results from the nanoindentation experiment (a) and the pressurized membrane experiment (d). The red-shift of the PL spectra vs. strain is visible along with the change of the lineshape indicating the exciton-to-trion conversion. (c,f) An illustration depicting the funneling of the free electrons in the spatially varying potential resulting from the non-uniform strain. The nanoindentation experiment induces the energy profile in (c) while the pressurized membrane results in the energy profile in (f). (b) An area scan of the trion/exciton ratio showing localized trion formation at the center of the suspended 2D monolayer, at the point of the highest strain. (e) Maps of the peak position for a triangular hole in the pressurized membrane experiment. The strain dependance of the PL in (d) was measured at the region of the highest shift. Sub-figures a,b,c reproduced with permission from Ref. [28]. Sub figures d,e reproduced with permission from Ref. [29].

The conversion of neutral excitons into negatively charged trion is a well-known feature of electrostatic gating. Once the free electrons density is increased through the electrostatic gating, the excitons have a high probability to bind to a free electron forming a trion.<sup>[45]</sup> Therefore, optical signatures of excitons to trions conversion that we observe is hinting that we effectively increase the free electron density in the region of high mechanical strain.

We can understand the underlying mechanism of the exciton-to-trion conversion by analyzing the drift-diffusion equation:<sup>[28]</sup>

$$\nabla(D\nabla n(r)) + \nabla(\mu n(r)\nabla u(r)) - \frac{n(r)}{\tau} - n^2(r)R_A + S(r) = 0 \quad (5)$$

where  $D$  is the diffusion coefficient,  $\mu$  is the mobility,  $u(r)$  is the potential due to the non-uniform strain,  $\tau$  is the lifetime,  $R_A$  is the Auger recombination rate, and  $S(r)$  is the generation term. Equation 5 is valid for all elementary excitations in the sample – free electrons, excitons and trions – and is solved for their corresponding densities. For the free electrons, the solution is simple as their lifetime is infinite and they have no Auger recombination and no generation term. In this case, the free electron density is  $n_{el}(r) \propto e^{-\frac{u(r)}{k_B T}}$  which is exactly the Boltzmann distribution in thermal equilibrium. This is a trivial and expected result and it means that the density of the electrons will be higher in the region of higher strain as depicted in Figure 4c,f. Since the density of the free electrons is higher at the points of high strain, we get an effective “mechanical doping” which explains the conversion of the neutral excitons into negatively charged trions. Strain-induced exciton-to-trion conversion has been observed in other works as well. “Mechanical doping” has been also demonstrated on a flexible substrate in WS<sub>2</sub> monolayer<sup>[42]</sup> as well in nanopillar-strained MoS<sub>2</sub>.<sup>[43]</sup>

So far only redistribution (or funneling) of the free carriers has been discussed, but what about excitons and trions funneling? From the numerical solution of Eq. 1, we find that the funneling efficiency, or the fraction of all excitons reaching the strain area, cannot exceed 4% at room temperature.<sup>[28]</sup>

Following the low reported exciton funneling efficiency, only 4%,<sup>[28]</sup> can we enhance this efficiency for large size monolayers ( $> 1 \mu\text{m}$ )? Can the solar cell envisioned in Ref. [8] be realized? To answer this question, we look again at Eq. 5. We see that the physical properties limiting the exciton diffusion length are the lifetime  $\tau$  and the Auger recombination  $R_A$ . It is hard to engineer the Auger recombination rate, but the lifetime can be controlled by moving from monolayers to heterostructures. In heterostructures, long-lived interlayer excitons can have a long ( $> 1 \mu\text{s}$ ) lifetime as electron and hole wavefunctions are spatially separated.<sup>[46–49]</sup> This can give the excitons enough time to reach the bottom of the potential contributing to a high funneling efficiency. This intuition is supported by the numerical evaluation of funneling efficiency

for a heterostructured sample.<sup>[44]</sup> In Figure 5 we see that depending on the diffusion coefficient (that can reach  $> 10 \text{ cm}^2/\text{s}$  in encapsulated samples<sup>[50]</sup>), the funneling efficiency can reach 50% efficiency,<sup>[44]</sup> at ambient temperatures.<sup>[44]</sup> This value is limited by thermodynamics as the Einstein relations suggest that high exciton mobility correspond to high diffusion.

### 3.4 Non-Uniform Strain in Graphene Phononic Crystals

Finally, we consider the effect of non-uniform strain on another quasiparticle – the phonon, and investigate perturbed phononic crystal.<sup>[24]</sup> Upon electrostatic gating (described in sec. 3) the device deforms out of plane (a) and the strain distribution becomes increasingly non-uniform as shown in a line cut in Figure 6b. This increasing non-uniformity perturbs the crystal order and affects the mechanical band gap gradually smearing it. To investigate in depth the effect of non-uniform strain, we plot the mechanical density of states (DOS) for various applied pressures in Figure 6c. At zero applied pressure, the bandgap is visible as a dip in the density of states, as within the bandgap no modes except a few localized modes are allowed. With increasing pressure two effects kick in: The band gap upshifts as the average strain within the system increases, and the band gap begins to smear out as the periodic order of the phononic crystal gets perturbed until it almost vanishes.

So far broadband tunable phononic crystal were only shown by means of simulation, yet experimental verification would be highly desirable. So how can one measure a

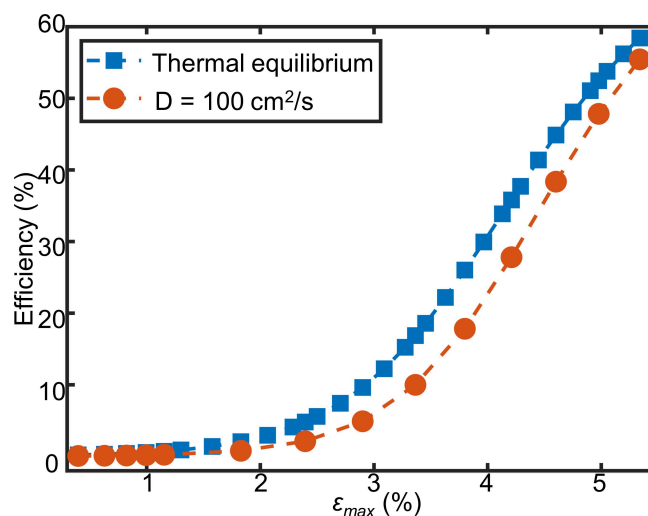


**Figure 5.** Exciton funneling efficiency vs. maximum strain calculated for a heterostructure with indirect exciton lifetime of  $1 \mu\text{s}$ , high diffusion coefficient of  $100 \text{ cm}^2/\text{s}$ , at 300 K, under solar illumination profile [44] (red circles). The funneling efficiency expected at thermal equilibrium for the same heterostructure (blue squares). Reproduced with permission from Ref. [44].

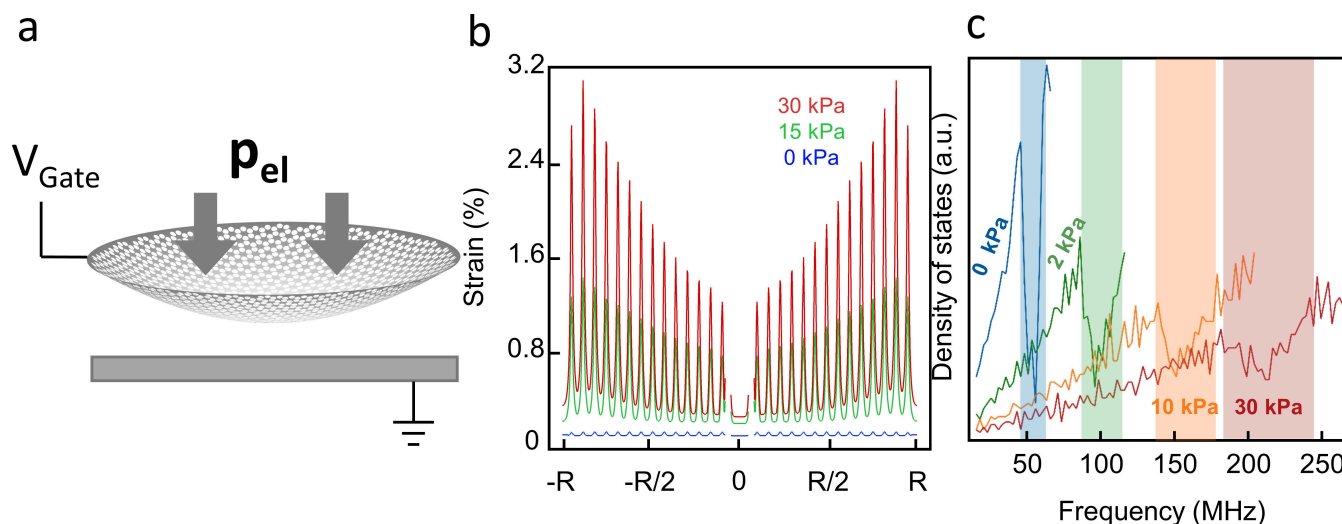


**Figure 6. Tunable graphene phononic crystal under non-uniform strain.** (a) An illustration of the out-of-plane deformation of the suspended phononic crystal under electrostatic pressure  $P$ . (b) Strain distribution in the device shown in (a) with increasing electrostatic pressure. Under higher pressure the distribution becomes increasingly non-uniform. (c) Calculated phononic density of states as a function of pressure applied to the suspended phononic crystal. The bandgap (marked by shaded areas) upshifts by more than 350%, while it starts to smear out as the phonic order gets perturbed due to the increasingly non-uniform strain distribution shown in (b). Reproduced with permission from Ref. [24].

phononic band structure or at least the bandgap? There are multiple possibilities. A very direct measurement is spatial mode mapping vs. frequency and subsequently assigning a wave-vector to each mode by Fourier-transformation.<sup>[51]</sup> With the known frequency one can then reproduce the band structure.<sup>[51,52]</sup> Yet this is only possible in very large samples due to spatial detection limits.<sup>[24]</sup> Another way is to measure transmission through a phononic sample.<sup>[15,16,53]</sup> To do so one needs an excitation on one side of the sample (e.g., via Surfaces Acoustic Waves or photo-thermally) and detects its motion on another side (e.g., interferometrical motion detection).<sup>[15,16,53]</sup> Here, the band gap acts as a stop band and significantly reduces transmission with it.<sup>[15,16,53]</sup> Finally, there is the option of an indirect detection. For example, one could search for a localized mode.<sup>[22,23]</sup> Such modes can only occur if there is a bandgap causing their localization. Also localized modes should be easily distinguished from other modes due to their enhanced quality factors resulting from reduced bending and radiation losses.<sup>[22,23]</sup>

#### 4. Conclusions

We have reviewed three different systems that are highly influenced by non-uniform strain. First, we considered pseudo-magnetic fields in graphene. As these fields arise in highly localized non-uniform strain nanostructures such as nanobubbles, nanopillars and nanoparticles, the Landau levels arising from pseudo-magnetic fields has been shown only through STM experiments.<sup>[39–42]</sup> There are proposals that pave the way to measure this effect in electrical devices<sup>[54]</sup> but it is

yet to be demonstrated experimentally, to the best of our knowledge.

Second, the non-uniform strain induces a “mechanical gating” effect that converts excitons to trions.<sup>[28,29]</sup> This effect is dominant when the lifetime of the excitons is too short and can be avoided when the strained 2D material is a heterostructure and the lifetimes of the excitons are on the order of  $1 \mu\text{s}$ .<sup>[44]</sup>

Last, we introduced the graphene-based phononic crystal that can be tuned via strain.<sup>[24]</sup> Here, strain non-uniformity smears the phononic bandgap. Frequency tunability via strain in phononic system is currently still a new feature and needs careful exploration. It is highly desirable as it opens the door for adjustable transfer of sound, heat and information.<sup>[14,55,56]</sup> Here it is noteworthy, that not only transmission amplitude, but also the transmission speed is adjustable.<sup>[24,52]</sup> A frequency-adjustable phononic system would give the possibility to dynamically couple to external degrees of freedom, as shown in the static case in Ref. [57]. Strain tunability in phononic devices opens the door to many exciting experiments as illustrated by the examples above. In summary, we believe that uniform and non-uniform strain engineering is emerging as powerful tool to control and study two-dimensional materials.

#### Acknowledgements

KB acknowledges generous support by DFG projects #449506295 and TRR 227. MGH acknowledges the Planning and Budgeting Committee (PBC) of the Council for Higher Education in Israel for the Vatav Fellowship for the recruitment of new faculty members in quantum technologies.

## References

- [1] R. Roldán et al., *J. Phys.-Condens. Mat.* **2015**, *27*, 313201.  
 [2] K. Liu et al., *Nano Lett.* **2014**, *14*, 5097.  
 [3] C. Lee et al., *Science* **2008**, *321*, 385.  
 [4] H. J. Conley et al., *Nano Lett.* **2013**, *13*, 3626.  
 [5] I. Niehues et al., *Nano Lett.* **2018**, *18*, 1751.  
 [6] F. Guinea, M. I. Katsnelson, A. K. Geim, *Nat. Phys.* **2009**, *6*, 30.  
 [7] T. Low and F. Guinea, *Nano Lett.* **2010**, *10*, 3551.  
 [8] J. Feng et al., *Nat. Photonics* **2012**, *6*, 866.  
 [9] E. Blundo et al., *Appl. Phys. Rev.* **2021**, *8*, 021318.  
 [10] Y. Wang et al., *Nano Res.* **2015**, *8*, 2562.  
 [11] R. K. Defo et al., *Phys. Rev. B* **2016**, *94*, 155310.  
 [12] D. Lloyd et al., *Nano Lett.* **2016**, *16*, 5836.  
 [13] M. S. Kushwaha et al., *Phys. Rev. Lett.* **1993**, *71*, 2022.  
 [14] M. Maldovan, *Nature* **2013**, *503*, 209.  
 [15] A. Khelif et al., *Appl. Phys. Lett.* **2004**, *84*, 4400.  
 [16] R. H. Olsson, I. El-Kady, *Meas. Sci. Technol.* **2008**, *20*, 012002.  
 [17] W. C. Jiang, Q. Lin, *Sci. Rep.* **2016**, *6*, 1.  
 [18] J. Zhao et al., *New J. Phys.* **2014**, *16*, 063031.  
 [19] S. Benchabane et al., *Phys. Rev. E* **2006**, *73*, 065601.  
 [20] S. Mohammadi et al., *Appl. Phys. Lett.* **2008**, *92*, 221905.  
 [21] P. E. Hopkins et al., *Nano Lett.* **2010**, *11*, 107.  
 [22] A. H. Ghadimi et al., *Science* **2018**, *360*, 764.  
 [23] Y. Tsaturyan et al., *Nat. Nanotechnol.* **2017**, *12*, 776.  
 [24] J. N. Kirchhof et al., *Nano Lett.* **2021**, *21*, 2174.  
 [25] V. Deinhart et al., *Beilstein J. Nanotech.* **2021**, *12*, 304.  
 [26] A. Castellanos-Gomez et al., *Nano Lett.* **2013**, *13*, 5361.  
 [27] A. V. Tyurnina et al., *ACS Photonics* **2019**, *6*, 516.  
 [28] M. G. Harats et al., *Nat. Photonics* **2020**, *14*, 5.  
 [29] S. Kovalchuk et al., *2D Mater.* **2020**, *7*, 035024.  
 [30] R. J. T. Nicholl et al., *Nat. Commun.* **2015**, *6*, 1.  
 [31] D. Vella, B. Davidovitch, *Soft Matter* **2017**, *13*, 2264.  
 [32] T. G. G. J. Chandler, D. Vella, *J. Mech. Phys. Solids* **2020**, *144*, 104109.  
 [33] E. Blundo et al., *Adv. Mater. Interfaces* **2020**, *7*, 2000621.  
 [34] D. Tedeschi et al., *Adv. Mater.* **2019**, *31*, 1903795.  
 [35] M. Dukic, J. D. Adams, G. E. Fantner, *Sci. Rep.* **2015**, *5*, 16393.  
 [36] G. López-Polín et al., *Carbon* **2017**, *124*, 42.  
 [37] A. P. Nayak et al., *Nano Lett.* **2014**, *15*, 346.  
 [38] G. J. Verbiest, S. Brinker, C. Stampfer, *Phys. Rev. B* **2015**, *92*, 075417.  
 [39] N. Levy et al., *Science* **2010**, *329*, 544.  
 [40] Y. Jiang et al., *Nano Lett.* **2017**, *17*, 2839.  
 [41] J. Mao et al., *Nature* **2020**, *584*, 215.  
 [42] C.-C. Hsu et al., *Sci. Adv.* **2020**, *6*.  
 [43] B. Zhu, X. Chen, X. Cui, *Sci. Rep.* **2015**, *5*, 9218.  
 [44] M. G. Harats, K. I. Bolotin, *2D Mater.* **2021**, *8*, 015010.  
 [45] J. S. Ross et al., *Nat. Commun.* **2013**, *4*, 1474.  
 [46] P. Nagler et al., *2D Mater.* **2017**, *4*, 025112.  
 [47] E. v. Calman et al., *Nat. Commun.* **2018**, *9*, 1895.  
 [48] H. Chen et al., *Nat. Commun.* **2016**, *7*, 12512.  
 [49] C. Jiang et al., *Nat. Commun.* **2018**, *9*, 1.  
 [50] J. Zipfel et al., *Phys. Rev. B* **2020**, *101*, 115430.  
 [51] R. Waitz et al., *Phys. Rev. B* **2012**, *85*, 035324.  
 [52] J. Cha, C. Daraio, *Nat. Nanotechnol.* **2018**, *13*, 1016.  
 [53] Y. Wang et al., *ACS Photonics* **2019**, *6*, 3225.  
 [54] E. Sela et al., *Phys. Rev. Lett.* **2020**, *124*, 026602.  
 [55] T. Vasileiadis et al., *J. Appl. Phys.* **2021**, *129*, 160901.  
 [56] D. Hatanaka, A. Bachtold, H. Yamaguchi, *Phys. Rev. Appl.* **2019**, *11*, 024024.  
 [57] R. A. Thomas et al., *Nat. Phys.* **2020**, *17*, 228.

Manuscript received: October 14, 2021

Revised manuscript received: November 23, 2021

Version of record online: February 25, 2022